Journal of Geophysical Research: Atmospheres

RESEARCH ARTICLE
10.1029/2018JD029323

Cold Tropical Pacific Sea Surface Temperatures During the Late Sixteenth-Century North American Megadrought

Benjamin I. Cook[1,2], A. Park Williams[3], Jason E. Smerdon[2], Jonathan G. Palmer[4], Edward R. Cook[3], David W. Stahle[5], and Sloan Coats[6]

[1]NASA Goddard Institute for Space Studies, New York, NY, USA, [2]Ocean and Climate Physics, Lamont-Doherty Earth Observatory, Palisades, NY, USA, [3]Tree-Ring Lab, Lamont-Doherty Earth Observatory, Palisades, NY, USA, [4]ARC Centre of Excellence for Australian Biodiversity and Heritage (CABAH), School of Biological, Earth and Environmental Sciences, University of New South Wales, Kensington, New South Wales, Australia, [5]Department of Geosciences, University of Arkansas, Fayetteville, AR, USA, [6]Woods Hole Oceanographic Institution, Woods Hole, MA, USA

Key Points:
- One of the most severe megadroughts in North America occurred in the late 16th-century
- We show this event occurred during a 25-year cold period in the tropical Pacific Ocean
- This provides evidence linking ocean forcing and megadroughts outside the Medieval Climate Anomaly

Supporting Information:
- Supporting Information S1
- Data Set S1
- Data Set S2
- Data Set S3

Correspondence to:
B. I. Cook,
benjamin.i.cook@nasa.gov

Citation:
Cook, B. I., Williams, A. P., Smerdon, J. E., Palmer, J. G., Cook, E. R., Stahle, D. W., & Coats, S. (2018). Cold tropical Pacific sea surface temperatures during the late sixteenth-century North American megadrought. *Journal Geophysical Research: Atmospheres*, *123*, 11,307–11,320. https://doi.org/10.1029/2018JD029323

Received 12 JUL 2018
Accepted 21 SEP 2018
Accepted article online 21 SEP 2018
Published online 16 OCT 2018

Abstract The late 16th-century North American megadrought was notable for its persistence, extent, intensity, and occurrence after the main interval of megadrought activity during the Medieval Climate Anomaly. Forcing from sea surface temperatures (SSTs) in the tropical Pacific is considered a possible driver of megadroughts, and we investigate this hypothesis for the late 16th-century event using two new 600-year long hydroclimate field reconstructions from Mexico and Australia. Areas represented by these reconstructions have strong teleconnections to tropical Pacific SSTs, evidenced by the leading principal component in each region explaining ~40% of local hydroclimate variability and correlating significantly with the boreal winter (December-January-February) NINO 3.4 index. Using these two principal components as predictors, we develop a skillful reconstruction of the December-January-February NINO 3.4 index. The reconstruction reveals that the late 16th-century megadrought likely occurred during one of the most persistent and intense periods of cold tropical Pacific SST anomalies of the last 600 years (1566–1590 C.E.; median NINO 3.4 = −0.79 K). This anomalously cold period coincided with a major filling episode for Kati Thanda-Lake Eyre in Australia, a hydroclimate response dynamically consistent with the reconstructed SST state. These results offer new evidence that tropical Pacific forcing was an important driver of the late 16th-century North American megadrought over the Southwest and Mexico, highlighting the large amplitude of natural variability that can occur within the climate system.

1. Introduction

Megadroughts, multidecadal intervals of drought more persistent than any event in the instrumental era, were ubiquitous features of North American climate during much of the last two millennia (E. R. Cook et al., 2004, 2016; Stahle et al., 2007; Stine, 1994; Woodhouse & Overpeck, 1998). One of the most persistent, widespread, and severe of these droughts occurred in the late 16th-century, extending across Mexico, the Southwest, Central Plains, Midwest, and the eastern United States (Stahle et al., 2000, 2007). This event stands out clearly in tree-ring based reconstructions of drought variability (e.g., Stahle et al., 2007), including the most recently updated version of the North American Drought Atlas (B. I. Cook, Cook, et al., 2016; Figure 1) which shows drought conditions affecting most of the Contiguous United States and northern Mexico during the late 1500s. The strongest anomalies were centered in the Southwest and Central Plains (dashed boxes), where the event is exceptionally intense and persistent compared to other droughts of the last 500 years (Figure 1; bottom two panels).

In addition to the tree-ring based North American Drought Atlas, the 16th-century megadrought is independently recorded in other climate proxies across North America. These include lake records in Michigan (Hupy & Yansa, 2009), Colorado (Routson et al., 2016), and Mexico (Metcalfe et al., 2010) and indicators of dune mobilization from the Central Plains (Forman et al., 2005; Halfen et al., 2012). This drought was severe enough to merit mention in historical documents from English and Spanish settlements in the eastern United States (Stahle et al., 2000), is cited as a likely reason for the abandonment of several Native American settlements in the Southwest United States (Schroeder, 1968), and contributed to an outbreak of hemorrhagic fever in 1576, an epidemic that caused ~2 million deaths in Mexico (Acuna-Soto et al., 2002). The drought also had

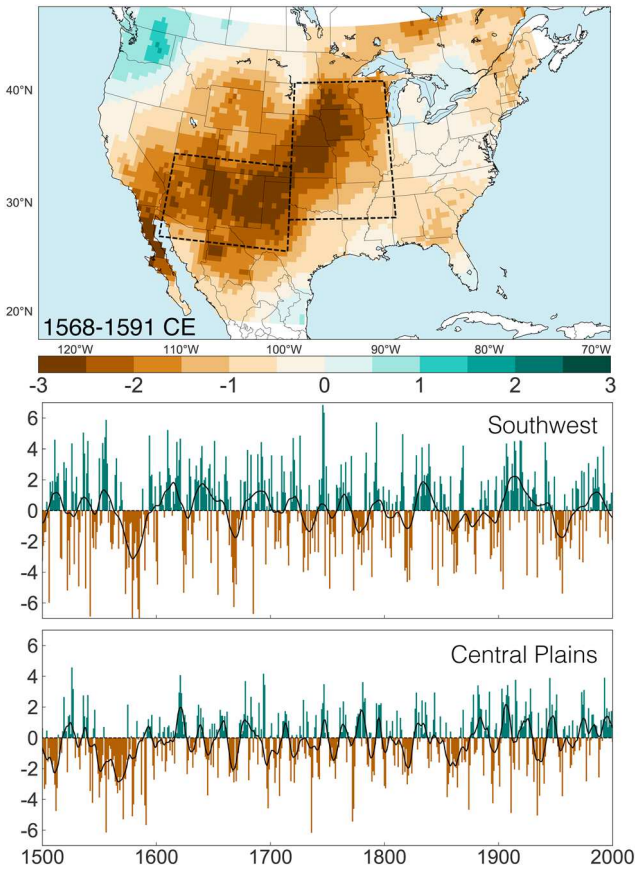

Figure 1. Summer (June-July-August) drought anomalies (Palmer Drought Severity Index) from the latest version of the North American Drought Atlas (B. I. Cook, Cook, et al., 2016) for the late 16th-century (top panel). In the North American Drought Atlas, the drought appears to have begun earlier in the Central Plains compared to the Southwest, consistent with previous tree-ring studies (Stahle et al., 2000), peaking in intensity over both regions during the 1570s and 1580s.

significant ecological impacts. Dune mobilization over the Central Plains, for example, is indicative of widespread vegetation mortality because mobilization only occurs when vegetation cover (and the associated stabilizing influence on the dunes) is lost due to moisture declines (Muhs & Maat, 1993; Muhs et al., 1996). Additionally, few living trees predate this megadrought in the Southwest, evidence for widespread tree mortality in the region at the time (P. M. Brown & Wu, 2005; Swetnam & Betancourt, 1998; Williams et al., 2013).

Decadal and longer periods of drought in Southwest North America and Mexico are often caused by persistent periods of cool sea surface temperatures (SSTs) in the eastern tropical Pacific (e.g., Delworth et al., 2015; Seager et al., 2005), typically associated with variability in the El Niño Southern Oscillation (ENSO). This is one of the leading hypotheses for earlier megadroughts during the Medieval Climate Anomaly (ca. 800–1300 C.E.; B. I. Cook, Cook, et al., 2016), with evidence from analyses using both process-based models (Coats, Smerdon, Cook, et al., 2015; Feng et al., 2008; Seager et al., 2008; Stevenson et al., 2015) and empirical approaches (Ault et al., 2018; Coats, Smerdon, Cook, et al., 2016; Coats, Smerdon, Karnauskas, et al., 2016). While these studies provide support for tropical Pacific SST forcing of megadroughts in these regions, few studies nevertheless have definitively attributed specific megadrought events to this mechanism (Coats, Smerdon, Cook, et al., 2016). In part, this is because there is little agreement across different reconstructions of ENSO and tropical Pacific SSTs over the last millennium (e.g., Coats, Smerdon, Cook, et al., 2016).

While the magnitude and impact of the late 16th-century megadrought has been widely investigated (see earlier references), no study has explicitly investigated the causes of this event, including the possible role of ENSO and tropical Pacific SSTs. Here we investigate this hypothesis using two recent paleoclimate reconstructions that offer new opportunities to evaluate tropical Pacific SST variability prior to the instrumental record: the Mexican Drought Atlas (MXDA, Stahle et al., 2016) and the Australia-New Zealand Drought Atlas (ANZDA, J. G. Palmer et al., 2015). These hydroclimate reconstructions exist in geographically distinct regions with strong teleconnections to the tropical Pacific. The MXDA and ANZDA are also spatially resolved, providing additional information by which to identify and validate fingerprints of tropical SST forcing in these data sets. Furthermore, the underlying proxies in both reconstructions primarily respond to moisture availability, and thus are more likely to be sensitive to tropical SST variability because of the larger influence of these dynamics on regional hydroclimate versus temperature. For this study, our primary research objectives are therefore to (1) quantify the influence of tropical Pacific SST variability in the MXDA and ANZDA during the historical period, (2) use this information to develop a reconstruction of the NINO 3.4 index for the last six centuries, and (3) determine the likely state of the tropical Pacific during the late 16th-century megadrought.

2. Methods

2.1. SST Data

The NINO 3.4 index is a widely used indicator of variability in tropical Pacific SSTs and ENSO, calculated for this study as the regional average SST anomaly over 120°W–170°W and 5°S–5°N from the Rayner et al. (2003) HadISST monthly SST data set (1870–present). The SST anomalies are calculated separately for each month relative to the baseline average from 1871 to 1970 C.E. The December-January-February (DJF; year centered on January) average anomalies from the NINO 3.4 index are shown in Figure 2. Blue-gray shading covers +0.5 to −0.5 K, the standard thresholds used to define El Niño or La Niña events. Strong El Niño (NINO 3.4 ≥ +1.0 K)

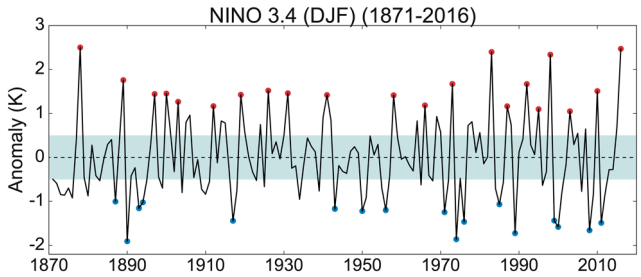

Figure 2. Seasonal average (DJF) NINO 3.4 index, calculated from the HadISST data set. Blue-gray shading indicates ±0.5 K, the typical thresholds used to define El Niño and La Niña events. Strong El Niño and La Niña events (defined as anomalies in excess of ±1 K) are indicated by the red and blue circles, respectively. DJF = December-January-February.

and La Niña (NINO 3.4 ≤ −1.0 K) events are highlighted in the red and blue dots, respectively. The HadISST data set is publicly and freely available from https://www.metoffice.gov.uk/hadobs/hadisst/.

2.2. Drought Atlases

The MXDA (Stahle et al., 2016) and ANZDA (J. G. Palmer et al., 2015) are tree-ring based reconstructions of the local summer self-calibrating Palmer Drought Severity Index (PDSI; W. C. Palmer 1965; Wells et al., 2004). PDSI is a measure of soil moisture drought, standardized to the local climate so that negative values indicate drier than normal conditions while positive values indicate wetter than normal conditions. The PDSI calculation itself integrates changes in moisture supply (precipitation) and demand (evapotranspiration) from the preceding months and seasons, with a persistence (typically 12 months or more) dependent on the regional climate (Wells et al., 2004). Variability in summer season PDSI in the reconstructions will thus reflect, to some degree, climate variability during the antecedent winter and spring. The reconstruction target for both drought atlases is the global instrumental PDSI data set of van der Schrier et al. (2013).

The regions targeted by these reconstructions have opposing responses to ENSO. El Niño events are generally wet over Mexico during the boreal cold season (November–April; Seager et al., 2009) and dry over eastern Australia during austral spring (September-October-November) and summer (DJF; Australian Bureau of Meteorology, 2014; Risbey et al., 2009). These anomalies are typically inverted during La Niña events. For both regions, other climate modes are also important drivers of hydroclimate variability. Positive phases of the Southern Annular Mode and atmospheric blocking centered near 140°E, for example, are both associated with wet conditions over much of eastern Australia during austral spring, one of the seasons of peak ENSO influence (Risbey et al., 2009). The Interdecadal Pacific Oscillation (IPO) also affects summer precipitation and drought over Australia, primarily by amplifying ENSO impacts when the two modes are in phase (e.g., a negative IPO and La Niña; Power et al., 1999). Similarly, positive/negative phases of the Indian Ocean Dipole cause dry/wet conditions across eastern Australia, with strongly amplified impacts when in-phase with ENSO (Risbey et al., 2009). Over Mexico, precipitation is also influenced by tropical Atlantic SSTs, with warm SSTs in this region typically causing dry conditions over northwest Mexico during November–April and enhancing precipitation in southern Mexico and Central America during May–October (Seager et al., 2009).

The MXDA (1400–2012 C.E.) uses 252 tree-ring proxies and targets boreal summer (June-July-August) average PDSI, covering all of Mexico and the southern United States up to 34.5°N. The tree-ring proxies that form the basis for the MXDA reconstruction are primarily sensitive to winter precipitation (Baek et al., 2017; St. George & Ault, 2014), the season of strongest ENSO teleconnections over the region (Ropelewski & Halpert, 1986). For the MXDA specifically, previous work has shown that the ENSO signal over the instrumental period is relatively strong and stable in Northern Mexico, but weaker and more nonstationary in southern Mexico where other influences are likely to be more important (Stahle et al., 2016). The reconstruction extends through 1985 C.E., after which it is merged with the instrumental PDSI from 1986 to 2012 C.E.

The ANZDA is a reconstruction of austral summer PDSI (DJF; year centered on January), covering eastern Australia, Tasmania, and New Zealand (J. G. Palmer et al., 2015), using 176 tree-ring chronologies and one coral luminescence record. The updated ANZDA (1400–2012 C.E.) analyzed in this study uses 22 additional tree-ring records, including several wood property chronologies from Tasmania that extend prior to 1500 C.E. (Allen et al., 2018), allowing for an extension of the reconstruction to 1400 C.E. to match the length of the MXDA. Additionally, all tree-ring records used in the updated ANZDA were standardized using signal-free standardization (Melvin & Briffa, 2008) to better preserve low-frequency variability. Despite relying primarily on nonlocal proxies, skillfulness of the ANZDA reconstruction over mainland Australia is comparable to, and by some measures even exceeds, the skill in other independent hydroclimate reconstructions of the region (B. I. Cook, Palmer et al., 2016). The DJF PDSI in the ANZDA is most sensitive to precipitation during the concurrent summer and preceding spring (B. I. Cook, Palmer et al., 2016), also the seasons when regional ENSO impacts are strongest (Risbey et al., 2009). Reconstructed values extend through 1975 C.E., merging with instrumental PDSI from 1976–2012 C.E. All data from the drought atlases used in this analysis have been uploaded as supporting information.

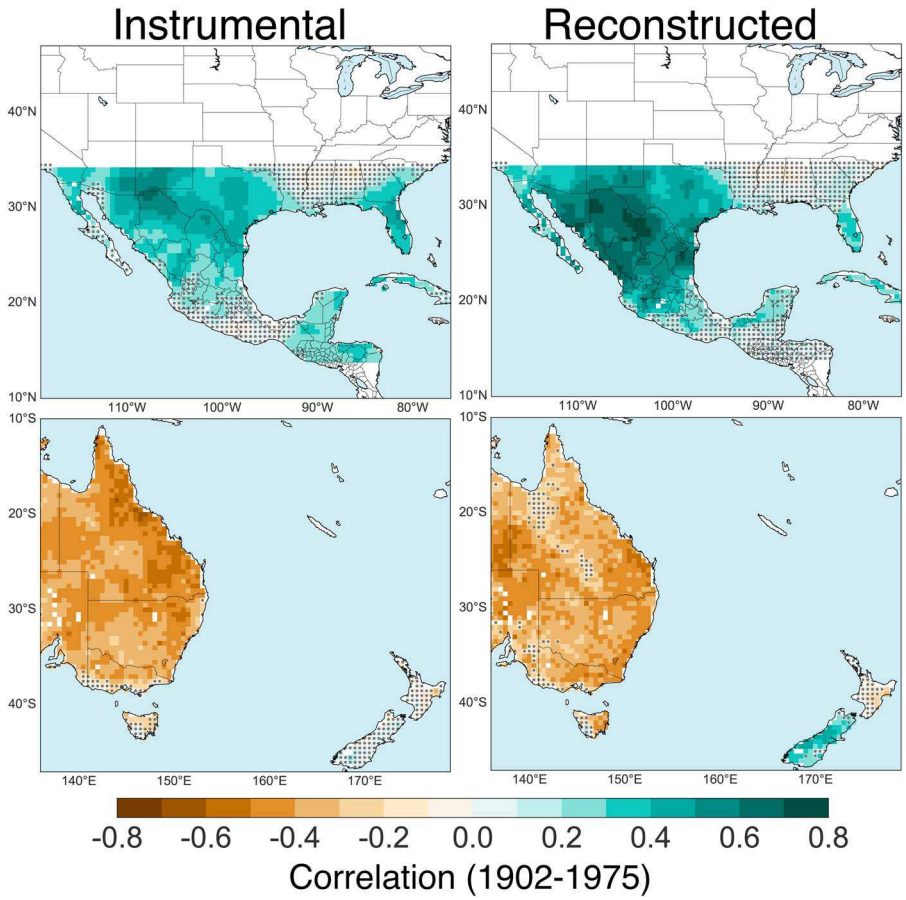

Figure 3. Pearson's correlations between the instrumental December-January-February NINO 3.4 index and the instrumental and reconstructed Palmer Drought Severity Index from the drought atlases (1902–1975). Insignificant correlations ($p > 0.05$) are masked by the gray stippling.

2.3. Analyses

All analyses are limited to 1400–1975 C.E., the common period of overlap in reconstructed PDSI across the two drought atlases. Prior to any analysis, the MXDA and ANZDA were recentered to a zero mean at each grid point for the same 100-year period used as the baseline in the instrumental NINO 3.4 record in Figure 1 (1871–1970 C.E.). This ensures that both drought atlases reflect variability around this common baseline. For the principal component analysis (PCA) specifically, we standardized the PDSI at each grid point to the mean and standard deviation calculated across all 576 years (1400–1975 C.E.).

The utility of the MXDA and ANZDA for reconstructing ENSO requires assessing and validating the spatiotemporal fingerprint of tropical Pacific SST variability in each drought atlas, which we quantify in several ways. First, we conduct point-by-point correlations between the instrumental DJF NINO 3.4 index and the instrumental and tree-ring reconstructed PDSI. Second, we composite average PDSI in the instrumental and tree-ring reconstructed PDSI for the strongest El Niño (NINO 3.4 $\geq +1.0$ K) and La Niña (NINO 3.4 ≤ -1.0 K) events, highlighting regions with the most consistent response. Finally, we conduct a PCA on the tree-ring reconstructed PDSI, comparing the leading principal components (PCs) against the NINO 3.4 index to identify the modes of variability most closely associated with tropical Pacific SSTs.

For the NINO 3.4 reconstruction itself, we use a composite-plus-scale approach (e.g., Smerdon et al., 2015), using PCs from the PCA that correlate significantly with the NINO 3.4 index (the leading PC from each drought atlas; see section 3 below). The reconstructed NINO 3.4 index is calculated as the Pearson's correlation weighted sum of these PCs, with the variance of the reconstruction scaled to match the calibration period variance of the instrumental NINO 3.4 time series. We use an ensemble split sample model calibration-validation procedure, using the PCs and instrumental NINO 3.4 time series from 1871 to 1975 C.E. At each step in the model calibration-validation, we use approximately half the data to fit the model parameters (Pearson's cor-

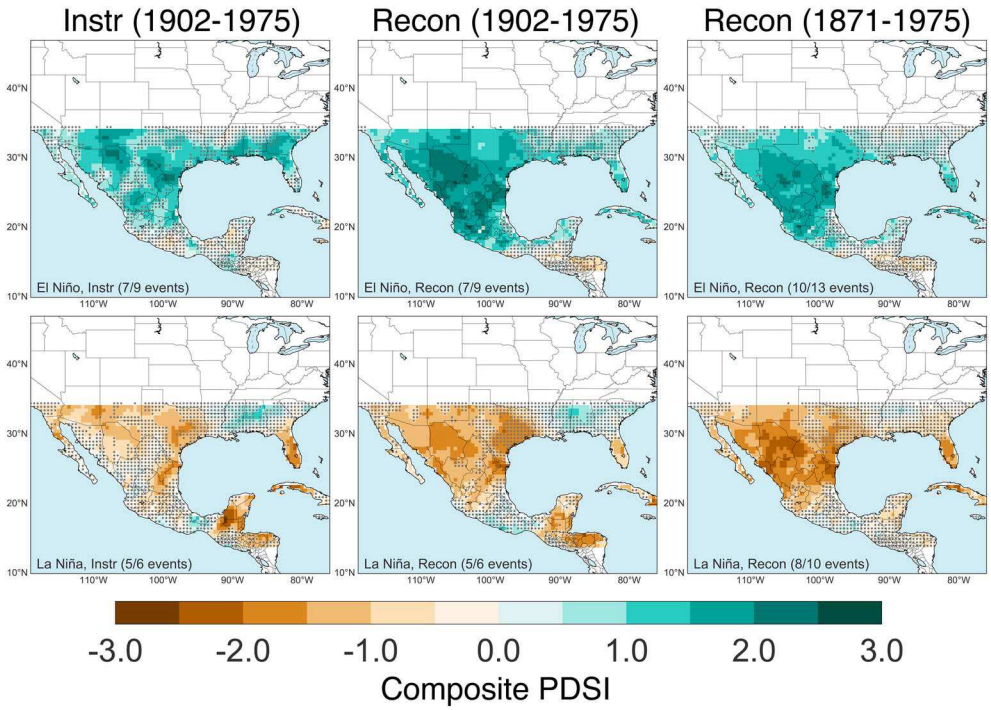

Figure 4. Composite average instrumental and reconstructed Mexican Drought Atlas PDSI during strong El Niño (NINO 3.4 ≥ +1.0 K) and La Niña (NINO 3.4 ≤ −1.0 K) events. Composites in the left and center columns are based on the same list of events from the common period of overlap between the instrumental and reconstructed PDSI records (1902–1975). For the reconstructed PDSI, the event list is expanded using all events from the full overlapping sea surface temperature record (1871–1975). Gray stippling indicates gridcells where <75% of individual years within the composite have the same sign as the composite average. PDSI = Palmer Drought Severity Index.

relations and variance; 51 years), with the remaining years (54) withheld for independent validation (using validation statistics described below). In each iteration, the calibration window moves forward 1 year in time (e.g., 1871–1921, 1872–1922 C.E., etc.) and all 54 remaining years are used for validation, yielding a total of 55 individual reconstructions.

To evaluate each individual reconstruction, we calculate Pearson's correlations between the instrumental and reconstructed NINO 3.4 indices separately for the calibration and validation windows. We also calculate the Reduction of Error (RE) and Coefficient of Efficiency (CE) statistics for the validation periods (E. R. Cook et al., 1994, 1999). The RE and CE statistics are much more conservative metrics of reconstruction skill because they compare the skill of the reconstruction during the validation period versus the mean of the instrumental observations from the calibration (RE) and validation (CE) intervals. RE and CE have theoretical ranges of $-\infty$ to +1, with positive values of these statistics indicating additional skill in the reconstruction beyond the climatology. CE is more rigorous than RE because CE evaluates the reconstruction relative to the mean from the independent validation period. RE will thus always exceed CE unless the means for the calibration and validation periods are equal. Following these evaluations, we generated a final reconstruction as the median values calculated across all 55 individual reconstructions.

One critical consideration in long-term analyses of tropical Pacific SST variability and regional climate is the often nonstationary nature of teleconnections between the two (Ashcroft et al., 2016; Coats, Smerdon, Seager, et al., 2015; Gallant et al., 2013; Lewis & LeGrande, 2015). These nonstationarities typically arise because of the influence of other factors on regional precipitation that may overwhelm or weaken correlations between local climate and these SSTs anomalies, including internal atmospheric variability or the influence of SSTs in other ocean basins. Precipitation over Mexico, for example, is highly sensitive to tropical Atlantic SSTs (Seager et al., 2009; Stahle et al., 2016), while over Australia phasing of the Indian Ocean Dipole and IPO both modulate the strength of ENSO impacts in the region (Cai et al., 2010; Power et al., 1999; Risbey et al., 2009). Shifts in the amplitude of ENSO variance may also affect teleconnection strengths (J. R. Brown et al., 2016; Coats et al., 2013). One motivation for using information from two independent and geographically separate data sets is

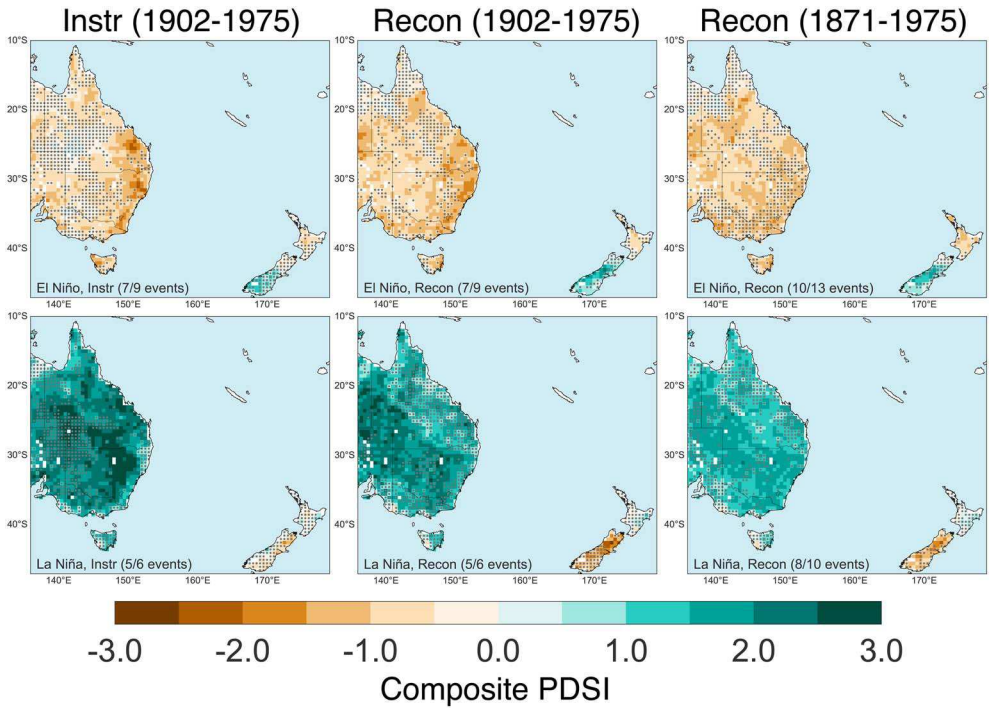

Figure 5. Composite average instrumental and reconstructed Australia-New Zealand Drought Atlas PDSI during strong El Niño (NINO 3.4 $\geq +1.0$ K) and La Niña (NINO 3.4 ≤ -1.0 K) events. Composites in the left and center columns are based on the same list of events from the common period of overlap between the instrumental and reconstructed PDSI records (1902–1975). For the reconstructed PDSI, the event list is expanded using all events from the full overlapping sea surface temperature record (1871–1975). Gray stippling indicates gridcells where <75% of individual years within the composite have the same sign as the composite average. PDSI = Palmer Drought Severity Index.

to minimize the potential influence of unstable teleconnections between ENSO and climate in any one region. Such an approach, where proxy information from multiple regions helps compensate for issues related to local nonstationarities, has been used in other climate index reconstructions (e.g., Lehner et al., 2012; McGregor et al., 2010).

3. Results

3.1. ENSO Variability in Instrumental and Reconstructed PDSI

From 1902 to 1975, the DJF NINO 3.4 index is strongly and significantly ($p \leq 0.05$) correlated with hydroclimate variability in the two drought atlases (Figure 3), consistent with previous analyses demonstrating the strong signal of many climate patterns in tree-ring based hydroclimate reconstructions (e.g., Baek et al., 2017). In the MXDA, correlations between the NINO 3.4 index and PDSI are stronger in the tree-ring based reconstruction compared to the instrumental PDSI, a result that may reflect lower meteorological data quality in Mexico prior to 1950 (Stahle et al., 2016). Correlations across northern and central Mexico generally exceed +0.60 in the reconstructed PDSI. By contrast, correlations between the NINO 3.4 index and the ANZDA reconstruction are modestly weaker compared to the instrumental PDSI, ranging mostly between +0.30 and +0.50 over much of eastern Australia.

The strength of the ENSO signal in the MXDA is also apparent in composite analyses (Figure 4), where we averaged PDSI during the strongest El Niño (NINO 3.4 $\geq +1.0$ K) and La Niña (NINO 3.4 ≤ -1.0 K) events (red and blue dots in Figure 1). To estimate robustness of the signal, we required that approximately 75% of the individual event years have the same sign as the composite average. Numbers in the lower right corners of the panels in Figures 4 and 5 indicate the total number of events (the denominator) and the number of events required to have the same sign as the composite mean to meet this 75% threshold (the numerator). Gridcells not reaching this threshold are masked with gray stippling. As with the correlation analysis, the ENSO signal is stronger in the reconstructed PDSI compared to the instrumental, with the most robust anomalies in northwest Mexico (Figure 4; left and center columns). When events from the extended instrumental SST record

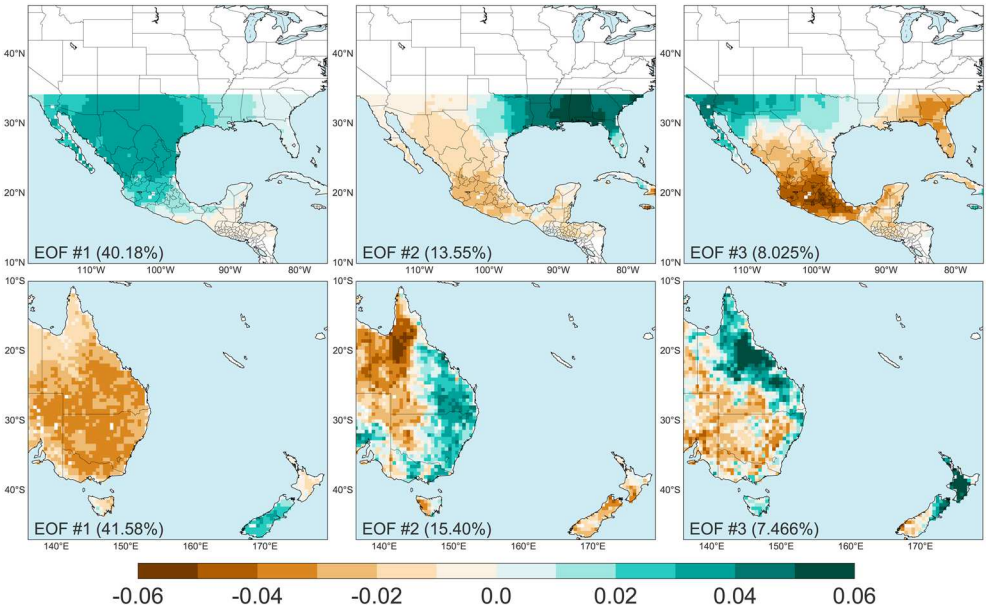

Figure 6. The first three EOFs from the independent principal component analyses of the Mexican Drought Atlas (top row) and Australia-New Zealand Drought Atlas (bottom row). Inset percentages indicate the percent of the total variance accounted by each EOF. EOF = empirical orthogonal function.

(back to 1871) are incorporated into the composite (Figure 4, right column) the results are similar, with slightly weaker magnitude of anomalies but nearly an identical spatial pattern. In all cases, the anomaly composite patterns for El Niño and La Niña have similar spatial patterns and absolute magnitudes, though they appear more robust in the El Niño composite, especially over Texas.

The same set of composites for the ANZDA highlights the asymmetrical nature of teleconnections and hydroclimate responses to El Niño versus La Niña over Australia and other regions (e.g., Cai et al., 2010, 2012; Hoerling et al., 1997; King et al., 2013; Power et al., 1999; Figure 5). Specifically, the intensity of hydroclimate anomalies over Australia is more strongly linked to large magnitude La Niña events than El Niños, as previously demonstrated in other studies (e.g., King et al., 2013). As with the MXDA, both the instrumental and reconstructed PDSI show similar spatial patterns and magnitudes of anomalies in the composites. The strongest and most robust drying during El Niño occurs along the east coast, while wetting during La Niña is more widespread across nearly all of eastern Australia (Figure 5; left and center columns). Results over this period are similar for both instrumental and reconstructed PDSI, though the La Niña wetting is more intense in the instrumental. When events are included from the pre-1900 period (Figure 5; right column), the intensity of the composite signal diminishes, especially for El Niño events, but the overall spatial patterns are the same.

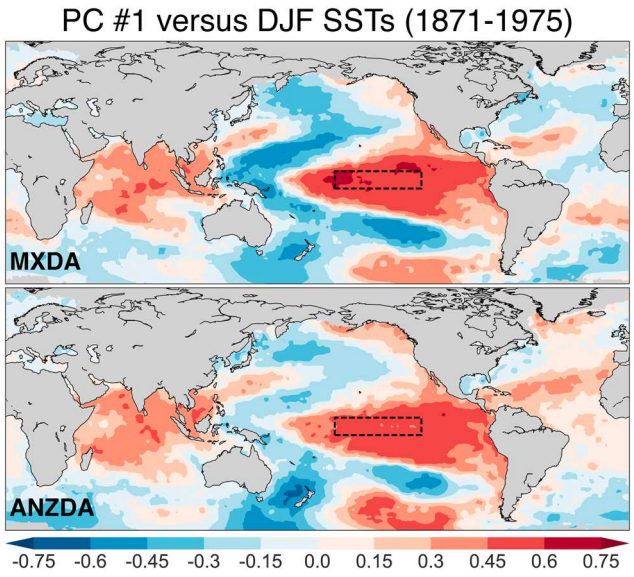

Figure 7. Correlations between the leading PCs from the MXDA (top panel) and ANZDA (bottom panel) and the DJF average SSTs in the HadISST data set (1871–1975). The NINO 3.4 region is outlined in the black dashed boxes. PC = principal component; DJF = December-January-February; SSTs = sea surface temperatures; MXDA = Mexican Drought Atlas; ANZDA = Australia-New Zealand Drought Atlas.

3.2. PCA

The empirical orthogonal functions (EOFs) from the first three leading modes are shown in Figure 6. The leading modes in the MXDA and ANZDA show coherent, same-signed anomalies across most of the domain, accounting for approximately 40% of the underlying variance in both data sets. For MXDA, EOF #2 has major opposing centers of action in the southeastern United States and southern Mexico, while EOF #3 has strongly opposing loci in the southwestern United States and Central/Southern Mexico. This EOF #3 has some superficial similarity to the *Mexican Dipole* pattern discussed in Stahle et al. (2016). Over ANZDA, EOF

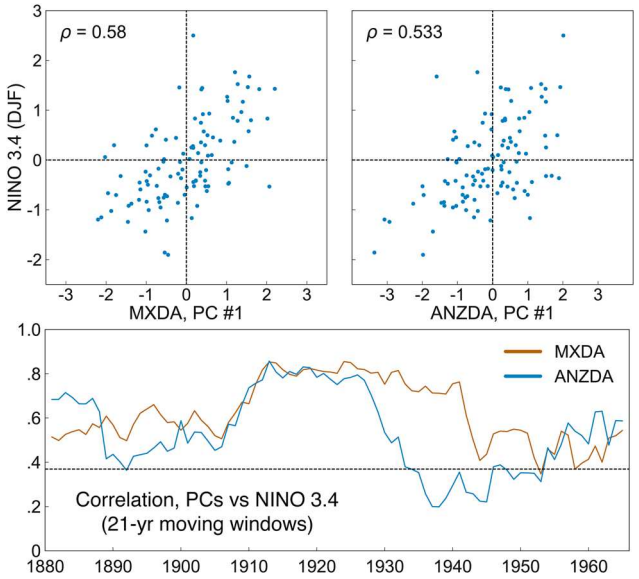

Figure 8. In the top panels, scatter plots and Pearson's correlations (1871–1975) between the DJF NINO 3.4 index and leading PCs (standardized to zero mean and unit standard deviation) from the MXDA and ANZDA. Bottom panel: moving window (21-year) correlations between the DJF NINO 3.4 index and the leading PCs for the same interval. For the moving window correlations, the one-sided significance threshold ($p \leq 0.05$) is indicated by the dashed black line. DJF = December-January-February; MXDA = Mexican Drought Atlas; ANZDA = Australia-New Zealand Drought Atlas; PC = principal component.

#2 is a zonal dipole, with contrasting anomalies between the coast and interior of eastern Australia, while EOF #3 shows antiphased anomalies between most of Queensland and the rest of mainland Australia.

The leading PC in each region correlates strongly (1871–1975 C.E.) with SSTs in the tropical Pacific and Indian Ocean (Figure 7) and the DJF NINO 3.4 index (Figure 8, top panels; $p < 0.001$). Over the entire period of overlap (1400–1975), the two PCs correlate significantly, but weakly, with each other (Pearson's $r = 0.34$, $p < 0.001$; Figure 9). The NINO 3.4 correlations are positive in both data sets, consistent with the expected hydroclimate response to tropical Pacific SST variability and the sign conventions of the associated EOFs. Moving window (21-year) correlations between the PCs and the NINO 3.4 index do show some periods of weaker correlation (Figure 8, bottom panel). The ANZDA shows the most pronounced weakening, dropping below a nominal 95th percentile significance threshold during the 1930s and 1940s. This was a time period of significantly weaker ENSO teleconnections over Australia, as noted in previous analyses of instrumental data from the region (Ashcroft et al., 2016; Power et al., 1999).

3.3. NINO 3.4 Reconstruction

Across our 55 individual reconstructions, the median Pearson's correlations between the instrumental and reconstructed DJF NINO 3.4 index for the calibration and validation periods were +0.72 (range from +0.55 to +0.79) and +0.62 (range from +0.55 to +0.75), respectively. The median validation period RE was +0.13, ranging from −0.20 to +0.57, with 44 of 55 calibration-validation intervals yielding positive RE values. The median CE was +0.06, ranging between −0.22 and +0.56, with 37 of 55 calibration-validation intervals yielding positive CE values. The weakest RE and CE statistics were generally found when calibrating on the earliest (pre-1880) part of the instrumental record. In aggregate, however, these statistics indicate a relatively stable and skillful reconstruction of the NINO 3.4 index using the leading PCs from the MXDA and ANZDA. The 55 individual (red lines) and finalized median (black line) NINO 3.4 reconstructions are shown in Figure 10.

The reconstruction shows a clear period of nearly continuous cold anomalies from 1566 to 1590 C.E., during which a marginally positive NINO 3.4 value only occurred in 1 year (1575 C.E.; +0.26 K). The median NINO 3.4 value for this 25-year interval in the final reconstruction is −0.79 K (mean of −0.85 K). This period includes one of the single coldest years in the reconstruction (1573 C.E.; −2.75 K), and the mean and median 25-year moving window NINO 3.4 anomalies centered in 1578 C.E. are the lowest compared to all other possible 25-year moving windows in the reconstruction (Figure 11). Other periods of intense and persistent cold SST anomalies occur elsewhere in the reconstruction, including during the early 1700s and the 1950s, though the latter appears much colder in the reconstruction than the instrumental data (Figure 10). The cold interval from 1566 to 1590 C.E. is a robust feature across the 55 individual reconstructions, ranging between −0.52 and −0.94 K. Further, persistent negative anomalies for this period are present in each of the individual predictor PCs (Figure 9), suggesting it is a relatively robust feature of the reconstruction and not dependent solely on one specific drought atlas and the stability of the associated teleconnections.

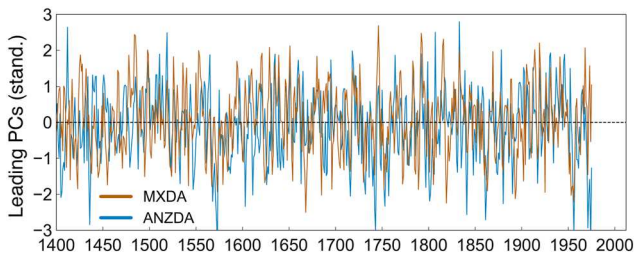

Figure 9. Leading PCs from the MXDA and ANZDA (1400–1975). PCs = principal components; MXDA = Mexican Drought Atlas; ANZDA = Australia-New Zealand Drought Atlas.

This reconstructed period of persistent cold conditions also overlaps with a major filling event for Kati Thanda-Lake Eyre in Australia, recorded in lake shoreline deposits in a reconstruction independent from the ANZDA (Cohen et al., 2018). Filling events for this mostly ephemeral lake basin occur during exceptionally wet years and in response to extreme rainfall events (Habeck-Fardy & Nanson, 2014). Notably, these filling events are most often associated with La Niña (Cohen et al., 2018; Habeck-Fardy & Nanson, 2014; Kotwicki & Allan, 1998), though the necessary precipitation can also derive from frontal systems connected to dynamics in the Indian

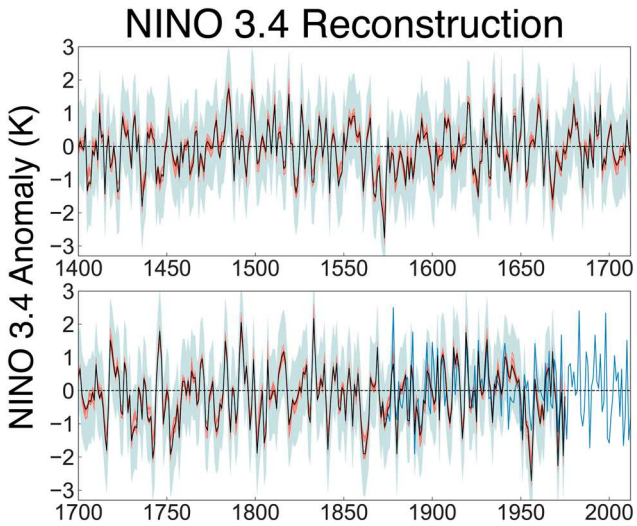

Figure 10. The 55 individual (red lines) and finalized median (black line) December-January-February NINO 3.4 composite-plus-scale reconstructions. Uncertainty estimates (blue-gray shading) are calculated as the 95th percentile prediction intervals from a regression between the instrumental and median reconstructed NINO 3.4 indices over 1871–1975 C.E. The instrumental NINO 3.4 index is shown in blue.

Ocean and the extratropics (Habeck-Fardy & Nanson, 2014). The date for the late 16th-century filling event is 1598 C.E., with dating errors (±36 years) that completely encompass the cold SST interval in our reconstruction, indicating likely overlap. Both the North American megadrought and Kati Thanda-Lake Eyre lake filling episode in Australia are dynamically consistent with what would be expected from a persistent period of cold conditions in the eastern tropical Pacific, providing additional support for this feature in our reconstruction.

Confidence in our reconstruction depends partially on tropical Pacific SST variability being the dominant driver of the antiphasing in hydroclimate between the MXDA and ANZDA. To test this, we averaged PDSI over southeast Australia in the ANZDA (141–155°E, 28–40°S) and northwest Mexico in the MXDA (110–100°W, 20–32°N). We then used these time series to calculate the frequency (over 1871–1975) of co-occurring wet conditions in the ANZDA and dry conditions in the MXDA (and vice versa) for different magnitudes of tropical Pacific SST and PDSI anomalies. These regions were chosen to have roughly the same area and represent the main centers of action for the PCs used as our predictors in the NINO 3.4 reconstruction. Regardless of the thresholds used, the frequency of simultaneous wet ANZDA/dry MXDA conditions is substantially higher during years with cold tropical Pacific SSTs (La Niña; Figure 12). During extreme cold events (NINO3.4 ≤ -1.0 K), for example, moderate and stronger wet conditions in southeastern Australia (PDSI $\geq +0.5$) and moderate and stronger dry conditions in northwest Mexico (PDSI ≤ -0.5) simultaneously occur in 8/10 years (0.8). For all other years, however, these anomalies only co-occur in 16/95 years (0.17). At the other extreme, intense wet conditions in the ANZDA (PDSI $\geq +1.0$) and intense drought in MXDA (PDSI ≤ -1.0) simultaneously occur during moderate or stronger La Niñas in 10/33 years (0.30), but are absent from any of the other 72 years in the record. We therefore conclude that tropical Pacific SST variability is the dominant driver of antiphasing in hydroclimate between the two regions.

3.4. Comparisons With Other ENSO Reconstructions

We compared our NINO 3.4 reconstruction derived from the drought atlases (hereafter, *DRGHT*) against several other ENSO reconstructions that use a diversity of methods and proxies. JEG (Emile-Geay et al., 2013) and Wilson (Wilson et al., 2010) are multiproxy reconstructions of the NINO 3.4 index, based primarily on corals and tree-ring series. Mann (Mann et al., 2009) is also a multiproxy reconstruction, but represents decadally smoothed SST anomalies from the NINO 3 region. Li (Li et al., 2013) and Cook (E. R. Cook et al., 2009) are tree-ring based reconstructions of the NINO 3.4 index. Coats (Coats, Smerdon, Cook, et al., 2016) is not a direct reconstruction of any ENSO index per se, but instead represents the decadal incidence of cold or warm ENSO conditions. In Coats, years are categorized as either El Niño (+1), La Niña (−1), or Neutral (0), and then a 10-year lowpass Butterworth filter is applied. For all comparisons with Mann or Coats, the other ENSO reconstructions were filtered in an identical manner.

Pairwise correlations across all seven reconstructions are positive over the common interval of overlap (1540–1975 C.E.; Figure 13). Correlations with DRGHT range from +0.30 (DRGHT versus Wilson) to +0.69 (DRGHT versus Cook). The strong correlation between DRGHT and Cook is somewhat expected, as the MXDA and the Cook reconstruction use many of the same tree-ring proxies from Mexico and the southwestern United States. Correlations between the other reconstructions range between +0.13 (Li versus Wilson) and +0.54 (Cook versus Li), indicating some weak to modest agreement while also highlighting the general lack of consensus in the literature regarding ENSO variability over the last several centuries. Despite these differences, all reconstructions show modestly cold conditions during 1566–1590 C.E., but with substantially different magnitudes and variability compared to DRGHT and each other (Figure 14). Of these, Cook (median NINO 3.4 = −0.56 K) is closest in magnitude to the intensity of cold conditions in DRGHT (median NINO 3.4 = −0.79 K), likely

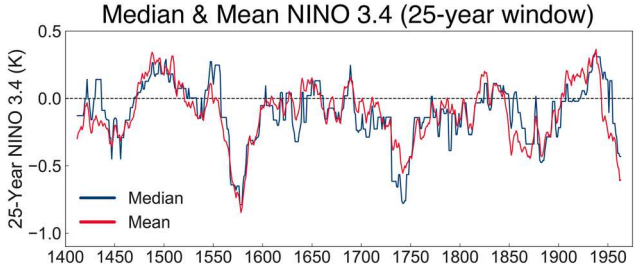

Figure 11. Median and mean NINO 3.4 values calculated from moving 25-year windows in the finalized median NINO 3.4 reconstruction.

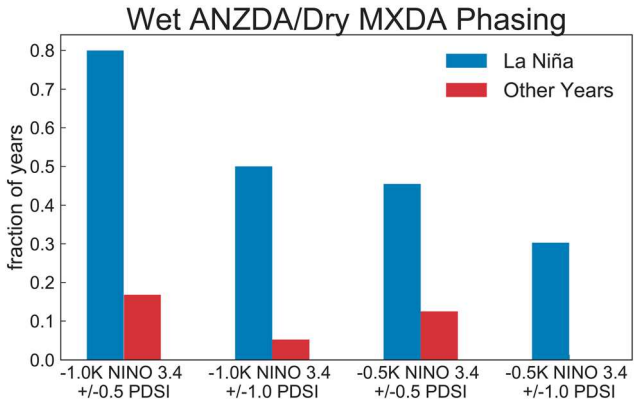

Figure 12. The fraction of years (1871–1975) in the drought reconstructions with co-occurring wet conditions in southeastern Australia (141–155°E, 28–40°S) and dry conditions in northwest Mexico (110–100°W, 20–32°N), for various NINO 3.4 and PDSI thresholds. Sample sizes range depending on NINO 3.4 threshold chosen: 10 La Niña years (95 other years) with NINO 3.4 ≤ −1.0 K and 33 La Niña years (72 other years) for NINO 3.4 ≤ −0.5 K. In all cases, the likelihood of simultaneously occurring wet conditions in southeastern Australia and dry conditions in northwest Mexico is substantially higher during cold events (La Niña) in the tropical Pacific. ANZDA = Australia-New Zealand Drought Atlas; MXDA = Mexican Drought Atlas; PDSI = Palmer Drought Severity Index.

also a consequence of the substantial proxy overlap between the two reconstructions. Coats does show a substantial extended cold interval of similar magnitude, but this occurs later in the 1580s and 1590s. For the other reconstructions, the magnitude of the cold anomaly during 1566–1590 C.E. ranges between −0.14 (JEG) and −0.26 K (Mann).

4. Discussion and Conclusions

Various hypotheses have been offered to explain the general occurrence of megadroughts in different regions of Western North America, including SST forcing from the tropical Pacific and Atlantic (Coats, Smerdon, Cook, et al., 2016; Feng et al., 2008; Seager et al., 2008), feedbacks from the land surface (B. I. Cook et al., 2013), and internal atmospheric variability (Stevenson et al., 2015). To date, however, few studies (e.g., Coats, Smerdon, Cook, et al., 2016) have attempted to attribute specific megadrought events to a particular cause. Here we used two new drought reconstructions in regions with strong teleconnections to the tropical Pacific to infer the state of ENSO and related SST variability during the late 16th-century megadrought. We find that this event occurred during the most intense multidecadal period (1566–1590 C.E.) of cold tropical Pacific SST anomalies

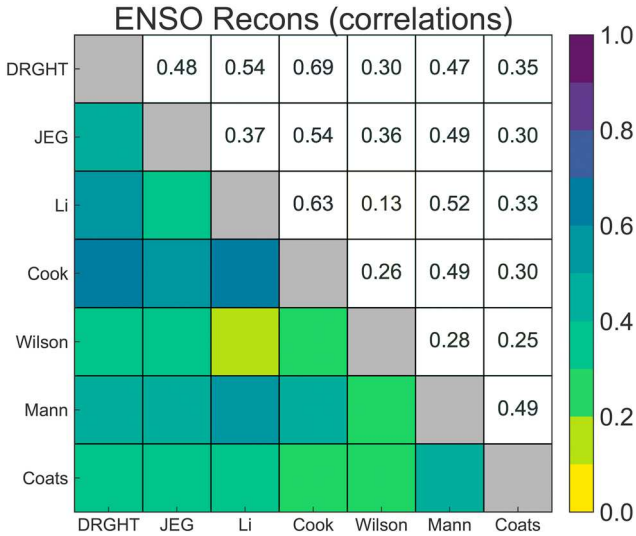

Figure 13. Correlations across various ENSO reconstructions and the reconstruction derived from the DRGHT. ENSO = El Niño Southern Oscillation; DRGHT = the NINO 3.4 reconstruction from the drought atlases.

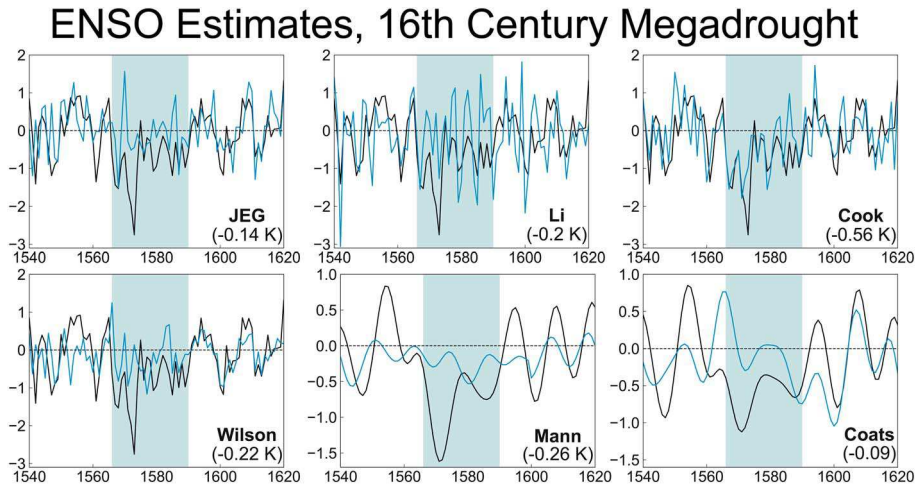

Figure 14. Comparisons of ENSO forcing from DRGHT and other reconstructions during the late 16th-century (shaded blue area; 1566–1590 C.E.). DRGHT is shown in each panel by the black line, and the other reconstructions are in blue. Magnitude of the ENSO anomaly (median) in each of the other reconstructions during 1566–1590 C.E. is indicated in the lower right corner of each panel. For comparisons with Mann, DRGHT was smoothed with a 10-year Butterworth lowpass filter. For comparisons with Coats, DRGHT was converted from sea surface temperature anomalies to an ENSO incidence series (using the same +1, −1, 0 scale as Coats), and then smoothed using a 10-year Butterworth lowpass filter. ENSO = El Niño Southern Oscillation; DRGHT = the NINO 3.4 reconstruction from the drought atlases.

of the last 600 years, suggesting an important role for ocean forcing of megadroughts even after the Medieval Climate Anomaly.

Our reconstruction shows colder conditions in the tropical Pacific during this interval compared to other ENSO reconstructions. However, there is only modest agreement across most tropical Pacific SST reconstructions over the last millennium, highlighting large uncertainties in our understanding of ocean variability during recent centuries. Development of SST reconstructions over the last millennium, including the tropical Pacific, is difficult because of the paucity of long-term, continuous marine proxies with seasonal or annual resolution (e.g., corals). Most efforts, including DRGHT and the other reconstructions we discussed, must therefore rely at least partially on terrestrial archives, with the resulting reconstruction dependent on the stability of teleconnections between the ocean basins and the local terrestrial climate recorded in these proxies. We attempted to mitigate some of these concerns by using two separate and geographically distant hydroclimate reconstructions centered in major regions of ENSO impacts. In this way, periods of weaker teleconnections in one region can theoretically be compensated if the signal in the other region is stronger. Use of terrestrial proxies can also cause circularity issues if the same records are used to simultaneously estimate and compare the terrestrial climate state (e.g., the megadrought) and the ocean background forcing (e.g., the ENSO reconstruction). However, in this study we do not use the MXDA to define any features of the late 16th-century megadrought (e.g., intensity, timing, etc.), and so this circularity is mitigated. Furthermore, while there is some overlap in tree-ring proxies used in the MXDA and other analyses of this megadrought (Stahle et al., 2000, 2007), this event is also independently recorded in other proxies and historical records (Forman et al., 2005; Halfen et al., 2012; Hupy & Yansa, 2009; Metcalfe et al., 2010; Routson et al., 2016; Stahle et al., 2000).

To more explicitly test the dependence of our reconstruction on the MXDA, we repeated the reconstruction procedure, but only using PC #1 from the ANZDA as a predictor. Validation period statistics in these more limited reconstructions were weaker (e.g., Pearson's r ranging from +0.43 to +0.69 and only 20 of the 55 reconstructions had positive RE and CE), but they generated a similar period of negative ENSO conditions from 1566 to 1590 C.E. (median NINO 3.4 during this interval ranged from −1.08 to −0.51 K across the 55 reconstructions). Such a result confirms that this extreme cold period does not depend on inclusion of the MXDA in the reconstruction, a similar result to Coats, Smerdon, Cook, et al., (2016) who were able to estimate ENSO states during North American megadroughts using information from drought reconstructions outside of North America (Monsoon Asia, Europe, and the Mediterranean). Given the independent information provided by the ANZDA in the NINO 3.4 reconstruction, and the fact that the MXDA was not used to identify or

characterize this megadrought, concerns regarding circularity are therefore largely immaterial to our main interpretations and conclusions.

While the persistent period of cold tropical Pacific SSTs in our reconstruction is a plausible driver of the late 16th-century megadrought in the Southwest and Mexico, it is unlikely to satisfactorily explain all features of this drought event, especially over the Central Plains. First, the drought over the Central Plains started earlier than both the drought over the Southwest and the period of persistent cold SSTs in our reconstruction (Figure 1). Second, teleconnections between drought over the Central Plains and tropical Pacific SSTs are relatively weak (Hoerling et al., 2009). It is therefore unlikely that the tropical Pacific was the main driver of the megadrought over this region. Central Plains hydroclimate, however, is sensitive to moisture transport from the Gulf of Mexico and SSTs in the tropical Atlantic (Nigam et al., 2011), leading to speculation that warm conditions in the tropical Atlantic may have contributed to megadroughts in this region (Coats, Smerdon, Karnauskas, et al., 2016; Feng et al., 2008). The Central Plains is also broadly considered a *hotspot* for land-atmosphere interactions (Koster et al., 2004, 2016); that is, a region where feedbacks from the land surface to the atmosphere are likely to be especially strong. Land-surface feedbacks have been demonstrated to be important for historical droughts over the Central Plains (e.g., the Dust Bowl; B. I. Cook et al., 2009; Schubert et al., 2004) and other research suggests they may have been important for megadroughts in the region too (B. I. Cook et al., 2013). The role of these and other mechanisms (e.g., internal atmospheric variability) during the 16th-century megadrought, however, remains to be explored.

Another major unresolved question is whether such a persistent, multidecadal period of cold eastern tropical Pacific SSTs arose through internal ocean-atmospheric variability or whether it could be externally forced. The late 16th-century occurs well after the Medieval Climate Anomaly, the period of most intense megadrought activity and relatively high radiative forcing. Several major eruptions did occur in the late 1500s, including Taal (1572 C.E.), Nevado del Ruiz (1595 C.E.), and Billy Mitchell (ca. 1580 C.E.). Most research to date, however, suggests that large volcanic eruptions favor the occurrence of El Niño events, rather than La Niña, (e.g., Emile-Geay et al., 2008; Khodri et al., 2017; Stevenson et al., 2016), an interpretation incompatible with the late 16th-century tropical Pacific SSTs in our reconstruction. The potential for internal ocean-atmosphere variability to generate such an extreme state can therefore not be rejected (e.g., Ault et al., 2018).

Regardless of the cause, the occurrence of such an extended cold period in our reconstruction demonstrates the capacity for the climate system during the preindustrial Common Era to generate extreme conditions from natural variability or forcings alone. Even in the face of greenhouse gas forced increases in aridity and drought risk (B. I. Cook et al., 2015; Cook, Palmer, et al., 2016; Seager et al., 2013), natural variability will still be important, especially in the near term (e.g., next several decades) when it has a strong potential to amplify or delay climate change forced trends (Delworth et al., 2015; Hawkins et al., 2015). The capacity of natural climate variability to impose extreme drought in the west thus still remains, and will be critical for interpreting projections of drought risk into the future.

Acknowledgments
B.I. Cook and A.P. Williams are supported by the NASA Modeling, Analysis, and Prediction program (NASA 80NSSC17K0265). A.P. Williams is also supported by NSF AGS 17-03029, Columbia University's center for Climate and Life, and the Vetlesen Foundation. D.W. Stahle is supported by NSF AGS-1266014. J.E. Smerdon is supported by AGS-1243204, AGS-1401400, and OISE-1743738. Lamont contribution 8261. Drought atlas data used in the analyses have been uploaded as supporting information.

References

Acuna-Soto, R., Stahle, D. W., Cleaveland, M. K., & Therrell, M. D. (2002). Megadrought and megadeath in 16th century Mexico. *Emerging Infectious Diseases*, *8*(4), 360–362.

Allen, K. J., Cook, E. R., Evans, R., Francey, R., Buckley, B. M., Palmer, J. G., et al. (2018). Lack of cool, not warm, extremes distinguishes late 20th century climate in 979-year Tasmanian summer temperature reconstruction. *Environmental Research Letters*, *13*(3), 034,041. https://doi.org/10.1088/1748-9326/aaafd7

Ashcroft, L., Gergis, J., & Karoly, D. J. (2016). Long-term stationarity of El Niño–Southern Oscillation teleconnections in southeastern Australia. *Climate Dynamics*, *46*(9), 2991–3006. https://doi.org/10.1007/s00382-015-2746-3

Ault, T. R., George, S. St., Smerdon, J. E., Coats, S., Mankin, J. S., Carrillo, C. M., et al. (2018). A robust null hypothesis for the potential causes of megadrought in western North America. *Journal of Climate*, *31*(1), 3–24. https://doi.org/10.1175/JCLI-D-17-0154.1

Australian Bureau of Meteorology (2014). What is El Niño and what might it mean for Australia? http://www.bom.gov.au/climate/updates/articles/a008-el-nino-and-australia.shtml

Baek, S. H., Smerdon, J. E., Coats, S., Williams, A. P., Cook, B. I., Cook, E. R., & Seager, R. (2017). Precipitation, temperature, and teleconnection signals across the combined North American, Monsoon Asia, and Old World Drought Atlases. *Journal of Climate*, *30*(18), 7141–7155. https://doi.org/10.1175/JCLI-D-16-0766.1

Brown, J. R., Hope, P., Gergis, J., & Henley, B. J. (2016). ENSO teleconnections with Australian rainfall in coupled model simulations of the last millennium. *Climate Dynamics*, *47*(1), 79–93. https://doi.org/10.1007/s00382-015-2824-6

Brown, P. M., & Wu, R. (2005). Climate and disturbance forcing of episodic tree recruitment in a southwestern ponderosa pine landscape. *Ecology*, *86*(11), 3030–3038. https://doi.org/10.1890/05-0034

Cai, W., van Rensch, P., Cowan, T., & Hendon, H. H. (2012). An asymmetry in the IOD and ENSO teleconnection pathway and its impact on Australian climate. *Journal of Climate*, *25*(18), 6318–6329. https://doi.org/10.1175/JCLI-D-11-00501.1

Cai, W., van Rensch, P., Cowan, T., & Sullivan, A. (2010). Asymmetry in ENSO teleconnection with regional rainfall, its multidecadal variability, and impact. *Journal of Climate*, *23*(18), 4944–4955.

Coats, S., Smerdon, J. E., Cook, B. I., & Seager, R. (2013). Stationarity of the tropical Pacific teleconnection to North America in CMIP5/PMIP3 model simulations. *Geophysical Research Letters*, *40*, 4927–4932. https://doi.org/10.1002/grl.50938

Coats, S., Smerdon, J. E., Cook, B. I., & Seager, R. (2015). Are simulated megadroughts in the North American Southwest forced? *Journal of Climate*, *28*(1), 124–142. https://doi.org/10.1175/JCLI-D-14-00071.1

Coats, S., Smerdon, J. E., Cook, B. I., Seager, R., Cook, E. R., & Anchukaitis, K. J. (2016). Internal ocean-atmosphere variability drives megadroughts in Western North America. *Geophysical Research Letters*, *43*, 9886–9894. https://doi.org/10.1002/2016GL070105

Coats, S., Smerdon, J. E., Karnauskas, K. B., & Seager, R. (2016). The improbable but unexceptional occurrence of megadrought clustering in the American West during the Medieval Climate Anomaly. *Environmental Research Letters*, *11*(7), 074025. https://doi.org/10.1088/1748-9326/11/7/074025

Coats, S., Smerdon, J. E., Seager, R., Griffin, D., & Cook, B. I. (2015). Winter-to-summer precipitation phasing in southwestern North America: A multicentury perspective from paleoclimatic model-data comparisons. *Journal of Geophysical Research: Atmospheres*, *120*, 8052–8064. https://doi.org/10.1002/2015JD023085

Cohen, T. J., Meyer, M. C., & May, J. H. (2018). Identifying extreme pluvials in the last millennia using optical dating of single grains of quartz from shorelines on Australia's largest lake. *The Holocene*, *28*(1), 150–165. https://doi.org/10.1177/0959683617715700

Cook, B. I., Ault, T. R., & Smerdon, J. E. (2015). Unprecedented 21st century drought risk in the American Southwest and Central Plains. *Science Advances*, *1*(1). https://doi.org/10.1126/sciadv.1400082

Cook, E. R., Briffa, K. R., & Jones, P. D. (1994). Spatial regression methods in dendroclimatology: A review and comparison of two techniques. *International Journal of Climatology*, *14*(4), 379–402. https://doi.org/10.1002/joc.3370140404

Cook, B. I., Cook, E. R., Smerdon, J. E., Seager, R., Williams, A. P., Coats, S., et al. (2016). North American megadroughts in the Common Era: reconstructions and simulations. *Wiley Interdisciplinary Reviews: Climate Change*, *7*, 411–432. https://doi.org/10.1002/wcc.394

Cook, E. R., D'Arrigo, R. D., & Anchukaitis, K. J. (2009). Tree ring 500 year ENSO index reconstructions. NOAA/NCDC Paleoclimatology Program.

Cook, E. R., Meko, D., Stahle, D., & Cleaveland, M. (1999). Drought reconstructions for the continental United States*. *Journal of Climate*, *12*(4), 1145–1162. https://doi.org/10.1175/1520-0442(1999)012<1145:DRFTCU>2.0.CO;2

Cook, B. I., Miller, R. L., & Seager, R. (2009). Amplification of the North American "Dust Bowl" drought through human-induced land degradation. *Proceedings of the National Academy of Sciences*, *106*(13), 4997–5001. https://doi.org/10.1073/pnas.0810200106

Cook, B. I., Palmer, J. G., Cook, E. R., Turney, C. S. M., Allen, K., Fenwick, P., et al. (2016). The paleoclimate context and future trajectory of extreme summer hydroclimate in eastern Australia. *Journal of Geophysical Research: Atmospheres*, *121*, 12,820–12,838. https://doi.org/10.1002/2016JD024892

Cook, B. I., Seager, R., Miller, R. L., & Mason, J. A. (2013). Intensification of North American megadroughts through surface and dust aerosol forcing. *Journal of Climate*, *26*, 4414–4430. https//10.1175/JCLI-D-12-00022.1

Cook, E. R., Woodhouse, C. A., Eakin, C. M., Meko, D. M., & Stahle, D. W. (2004). Long-term aridity changes in the western United States. *Science*, *306*(5698), 1015–1018. https://doi.org/10.1126/science.1102586

Delworth, T. L., Zeng, F., Rosati, A., Vecchi, G. A., & Wittenberg, A. T. (2015). A link between the hiatus in global warming and North American drought. *Journal of Climate*, *28*(9), 3834–3845. https://doi.org/10.1175/JCLI-D-14-00616.1

Emile-Geay, J., Cobb, K. M., Mann, M. E., & Wittenberg, A. T. (2013). Estimating central equatorial Pacific SST variability over the past millennium. Part 2: Reconstructions and implications. *Journal of Climate*, *26*, 2329–2352. https://doi.org/10.1175/JCLI-D-11-00510.1

Emile-Geay, J., Seager, R., Cane, M. A., Cook, E. R., & Haug, G. H. (2008). Volcanoes and ENSO over the past millennium. *Journal of Climate*, *21*(13), 3134–3148. https://doi.org/10.1175/2007JCLI1884.1

Feng, S., Oglesby, R. J., Rowe, C. M., Loope, D. B., & Hu, Q. (2008). Atlantic and Pacific SST influences on Medieval drought in North America simulated by the Community Atmospheric Model. *Journal of Geophysical Research*, *113*(D11). https://doi.org/10.1029/2007JD009347

Forman, S. L., Marin, L., Pierson, J., Gomez, J., Miller, G. H., & Webb, R. S. (2005). Aeolian sand depositional records from western Nebraska: Landscape response to droughts in the past 1500 years. *The Holocene*, *15*(7), 973–981. https://doi.org/10.1191/0959683605hl871ra

Gallant, A. J. E., Phipps, S. J., Karoly, D. J., Mullan, A. B., & Lorrey, A. M. (2013). Nonstationary Australasian teleconnections and implications for paleoclimate reconstructions. *Journal of Climate*, *26*(22), 8827–8849. https://doi.org/10.1175/JCLI-D-12-00338.1

Habeck-Fardy, A., & Nanson, G. C. (2014). Environmental character and history of the Lake Eyre Basin, one seventh of the Australian continent. *Earth-Science Reviews*, *132*, 39–66. https://doi.org/10.1016/j.earscirev.2014.02.003

Halfen, A. F., Johnson, W. C., Hanson, P. R., Woodburn, T. L., Young, A. R., & Ludvigson, G. A. (2012). Activation history of the Hutchinson dunes in east-central Kansas, USA during the past 2200 years. *Aeolian Research*, *5*, 9–20. https://doi.org/10.1016/j.aeolia.2012.02.001

Hawkins, E., Smith, R. S., Gregory, J. M., & Stainforth, D. A. (2015). Irreducible uncertainty in near-term climate projections. *Climate Dynamics*, 3807–3819. https://doi.org/10.1007/s00382-015-2806-8

Hoerling, M. P., Kumar, A., & Zhong, M. (1997). El Niño, La Niña, and the nonlinearity of their teleconnections. *Journal of Climate*, *10*(8), 1769–1786. https://doi.org/10.1175/1520-0442(1997)010<1769:ENOLNA>2.0.CO;2

Hoerling, M., Quan, X. W., & Eischeid, J. (2009). Distinct causes for two principal US droughts of the 20th century. *Geophysical Research Letters*, *36*, L19708. https://doi.org/10.1029/2009GL039860

Hupy, C. M., & Yansa, C. H. (2009). Late Holocene vegetation history of the forest tension zone in central Lower Michigan, USA. *Physical Geography*, *30*(3), 205–235. https://doi.org/10.2747/0272-3646.30.3.205

Khodri, M., Izumo, T., Vialard, J., Janicot, S., Cassou, C., Lengaigne, M., et al. (2017). Tropical explosive volcanic eruptions can trigger El Niño by cooling tropical Africa. *Nature Communications*, *8*(1), 778. https://doi.org/10.1038/s41467-017-00755-6

King, A. D., Alexander, L. V., & Donat, M. G. (2013). Asymmetry in the response of eastern Australia extreme rainfall to low-frequency Pacific variability. *Geophysical Research Letters*, *40*, 2271–2277. https://doi.org/10.1002/grl.50427

Koster, R. D., Chang, Y., Wang, H., & Schubert, S. D. (2016). Impacts of local soil moisture anomalies on the atmospheric circulation and on remote surface meteorological fields during boreal summer: A comprehensive analysis over North America. *Journal of Climate*, *29*(20), 7345–7364. https://doi.org/10.1175/JCLI-D-16-0192.1

Koster, R. D., Dirmeyer, P. A., Guo, Z., Bonan, G., Chan, E., Cox, P., et al. (2004). Regions of strong coupling between soil moisture and precipitation. *Science*, *305*(5687), 1138–1140. https://doi.org/10.1126/science.1100217

Kotwicki, V., & Allan, R. (1998). La Niña de Australia—Contemporary and palaeo-hydrology of Lake Eyre. *Palaeogeography, Palaeoclimatology, Palaeoecology*, *144*(3), 265–280. https://doi.org/10.1016/S0031-0182(98)00122-9

Lehner, F., Raible, C. C., & Stocker, T. F. (2012). Testing the robustness of a precipitation proxy-based North Atlantic Oscillation reconstruction. *Quaternary Science Reviews*, *45*, 85–94. https://doi.org/10.1016/j.quascirev.2012.04.025

Lewis, S. C., & LeGrande, A. N. (2015). Stability of ENSO and its tropical Pacific teleconnections over the Last Millennium. *Climate of the Past*, *11*(10), 1347–1360. https://doi.org/10.5194/cp-11-1347-2015

Li, J., Xie, S.-P., Cook, E. R., Morales, M. S., Christie, D. A., Johnson, N. C., et al. (2013). El Niño modulations over the past seven centuries. *Nature Climate Change*, *3*(9), 822–826. https://doi.org/10.1038/nclimate1936
Mann, M. E., Zhang, Z., Rutherford, S., Bradley, R. S., Hughes, M. K., Shindell, D., et al. (2009). Global signatures and dynamical origins of the Little Ice Age and Medieval Climate Anomaly. *Science*, *326*(5957), 1256–1260. https://doi.org/10.1126/science.1177303
McGregor, S., Timmermann, A., & Timm, O. (2010). A unified proxy for ENSO and PDO variability since 1650. *Climate of the Past*, *6*(1), 1–17. https://doi.org/10.5194/cp-6-1-2010
Melvin, T. M., & Briffa, K. R. (2008). A "signal-free" approach to dendroclimatic standardisation. *Dendrochronologia*, *26*(2), 71–86. https://doi.org/10.1016/j.dendro.2007.12.001
Metcalfe, S. E., Jones, M. D., Davies, S. J., Noren, A., & MacKenzie, A. (2010). Climate variability over the last two millennia in the North American Monsoon region, recorded in laminated lake sediments from Laguna de Juanacatlán, Mexico. *The Holocene*, *20*(8), 1195–1206. https://doi.org/10.1177/0959683610371994
Muhs, D. R., & Maat, P. B. (1993). The potential response of eolian sands to greenhouse warming and precipitation reduction on the Great Plains of the USA. *Journal of Arid Environments*, *25*(4), 351–361. https://doi.org/10.1006/jare.1993.1068
Muhs, D. R., Stafford, T. W., Cowherd, S. D., Mahan, S. A., Kihl, R., Maat, P. B., et al. (1996). Origin of the late Quaternary dune fields of northeastern Colorado. *Geomorphology*, *17*(1–3), 129–149. https://doi.org/10.1016/0169-555X(95)00100-J
Nigam, S., Guan, B., & Ruiz-Barradas, A. (2011). Key role of the Atlantic multidecadal oscillation in 20th century drought and wet periods over the Great Plains. *Geophysical Research Letters*, *38*, L16713. https://doi.org/10.1029/2011GL048650
Palmer, W. C. (1965). Meteorological drought (*Research Paper No. 45*). Washington, DC: US Weather Bureau. 58.
Palmer, J. G., Cook, E. R., Turney, C. S. M., Allen, K., Fenwick, P., Cook, B. I., et al. (2015). Drought variability in the eastern Australia and New Zealand summer drought atlas (ANZDA, CE 1500–2012) modulated by the Interdecadal Pacific Oscillation. *Environmental Research Letters*, *10*(12), 124002. https://doi.org/10.1088/1748-9326/10/12/124002
Power, S., Casey, T., Folland, C., Colman, A., & Mehta, V. (1999). Inter-decadal modulation of the impact of ENSO on Australia. *Climate Dynamics*, *15*(5), 319–324. https://doi.org/10.1007/s003820050284
Rayner, N. A., Parker, D. E., Horton, E. B., Folland, C. K., Alexander, L. V., Rowell, D. P., et al. (2003). Global analyses of sea surface temperature, sea ice, and night marine air temperature since the late nineteenth century. *Journal of Geophysical Research*, *108*, 4407. https://doi.org/10.1029/2002JD002670
Risbey, J. S., Pook, M. J., McIntosh, P. C., Wheeler, M. C., & Hendon, H. H. (2009). On the remote drivers of rainfall variability in Australia. *Monthly Weather Review*, *137*(10), 3233–3253. https://doi.org/10.1175/2009MWR2861.1
Ropelewski, C. F., & Halpert, M. S. (1986). North American precipitation and temperature patterns associated with the El Niño/Southern Oscillation (ENSO). *Monthly Weather Review*, *114*(12), 2352–2362. https://doi.org/10.1175/1520-0493(1986)114<2352:NAPATP>2.0.CO;2
Routson, C. C., Overpeck, J. T., Woodhouse, C. A., & Kenney, W. F. (2016). Three millennia of southwestern North American dustiness and future implications. *PloS One*, *11*(2), E0149573. https://doi.org/10.1371/journal.pone.0149573
Schroeder, A. H. (1968). Shifting for survival in the Spanish Southwest. *New Mexico Historical Review*, *43*(4), 291.
Schubert, S. D., Suarez, M. J., Pegion, P. J., Koster, R. D., & Bacmeister, J. T. (2004). On the cause of the 1930s Dust Bowl. *Science*, *303*(5665), 1855–1859. https://doi.org/10.1126/science.1095048
Seager, R., Burgman, R., Kushnir, Y., Clement, A., Cook, E., Naik, N., & Miller, J. (2008). Tropical Pacific forcing of North American medieval megadroughts: Testing the concept with an atmosphere model forced by coral-reconstructed SSTs. *Journal of Climate*, *21*(23), 6175–6190. https://doi.org/10.1175/2008JCLI2170.1
Seager, R., Kushnir, Y., Herweijer, C., Naik, N., & Velez, J. (2005). Modeling of tropical forcing of persistent droughts and pluvials over western North America: 1856–2000. *Journal of Climate*, *18*(19), 4065–4088. https://doi.org/10.1175/JCLI3522.1
Seager, R., Ting, M., Davis, M., Cane, M., Naik, N., Nakamura, J., et al. (2009). Mexican drought: An observational modeling and tree ring study of variability and climate change. *Atmósfera*, *22*(1), 1–31.
Seager, R., Ting, M., Li, C., Naik, N., Cook, B., Nakamura, J., & Liu, H. (2013). Projections of declining surface-water availability for the southwestern United States. *Nature Climate Change*, *3*, 482–486. https://doi.org/10.1038/nclimate1787
Smerdon, J. E., Cook, B. I., Cook, E. R., & Seager, R. (2015). Bridging past and future climate across paleoclimatic reconstructions, observations, and models: A hydroclimate case study. *Journal of Climate*, *28*(8), 3212–3231. https://doi.org/10.1175/JCLI-D-14-00417.1
St. George, S., & Ault, T. R. (2014). The imprint of climate within Northern Hemisphere trees. *Quaternary Science Reviews*, *89*, 1–4. https://doi.org/10.1016/j.quascirev.2014.01.00
Stahle, D. W., Cook, E. R., Burnette, D. J., Villanueva, J., Cerano, J., Burns, J. N., et al. (2016). The Mexican Drought Atlas: Tree-ring reconstructions of the soil moisture balance during the late pre-Hispanic, colonial, and modern eras. *Quaternary Science Reviews*, *149*, 34–60. https://doi.org/10.1016/j.quascirev.2016.06.018
Stahle, D. W., Cook, E. R., Cleaveland, M. K., Therrell, M. D., Meko, D. M., Grissino-Mayer, H. D., et al. (2000). Tree-ring data document 16th century megadrought over North America. *Eos, Transactions American Geophysical Union*, *81*(12), 121–125. https://doi.org/10.1029/00EO00076
Stahle, D. W., Fye, F. K., Cook, E. R., & Griffin, R. D. (2007). Tree-ring reconstructed megadroughts over North America since AD 1300. *Climatic Change*, *83*(1), 133–149. https://doi.org/10.1007/s10584-006-9171-x
Stevenson, S., Otto-Bliesner, B., Fasullo, J., & Brady, E. (2016). "El Niño Like" hydroclimate responses to last millennium volcanic eruptions. *Journal of Climate*, *29*(8), 2907–2921. https://doi.org/10.1175/JCLI-D-15-0239.1
Stevenson, S., Timmermann, A., Chikamoto, Y., Langford, S., & DiNezio, P. (2015). Stochastically generated North American megadroughts. *Journal of Climate*, *28*(5), 1865–1880. https://doi.org/10.1175/JCLI-D-13-00689.1
Stine, S. (1994). Extreme and persistent drought in California and Patagonia during mediaeval time. *Nature*, *369*(6481), 546–549. https://doi.org/10.1038/369546a0
Swetnam, T. W., & Betancourt, J. L. (1998). Mesoscale disturbance and ecological response to decadal climatic variability in the American Southwest. *Journal of Climate*, *11*(12), 3128–3147. https://doi.org/10.1175/1520-0442(1998)011<3128:MDAERT>2.0.CO;2
van der Schrier, G., Barichivich, J., Briffa, K. R., & Jones, P. D. (2013). A scPDSI-based global data set of dry and wet spells for 1901–2009. *Journal of Geophysical Research: Atmospheres*, *118*, 4025–4048. https://doi.org/10.1002/jgrd.50355
Wells, N., Goddard, S., & Hayes, M. J. (2004). A self-calibrating Palmer drought severity index. *Journal of Climate*, *17*(12), 2335–2351. https://doi.org/10.1175/1520-0442(2004)017<2335:ASPDSI>2.0.CO;2
Williams, A. P., Allen, C. D., Macalady, A. K., Griffin, D., Woodhouse, C. A., Meko, D. M., et al. (2013). Temperature as a potent driver of regional forest drought stress and tree mortality. *Nature Climate Change*, *3*(3), 292–297. https://doi.org/10.1038/nclimate1693
Wilson, R., Cook, E., D'Arrigo, R., Riedwyl, N., Evans, M. N., Tudhope, A., & Allan, R. (2010). Reconstructing ENSO: The influence of method, proxy data, climate forcing and teleconnections. *Journal of Quaternary Science*, *25*(1), 62–78. https://doi.org/10.1002/jqs.1297
Woodhouse, C. A., & Overpeck, J. T. (1998). 2000 years of drought variability in the central United States. *Bulletin of the American Meteorological Society*, *79*(12), 2693–2714. https://doi.org/10.1175/1520-0477(1998)079<2693:YODVIT>2.0.CO;2